AERODYNAMICS, PERFORMANCE AND CONTROL OF AIRPLANES IN FORMATION FLIGHT*)

Markus Beukenberg, Dietrich Hummel
Institut für Strömungsmechanik, Technische Universität Braunschweig
Bienroder Weg 3, D - 3300 Braunschweig

Abstract

Formation flight is widely used by migrating birds. Each wing flies in an upwash field generated by all other wings of the formation, which leads to a reduction in flight power demand for each wing as well as for the whole formation. In this paper the technical realisation of this principle is analyzed by means of theoretical aerodynamics, by flight tests on the performance characteristics and by the application of an automatic control system in formation flights. In formations of two airplanes Do-28 a maximum flight power reduction of about 15% is achievable for the rear aircraft at very small lateral distances. The flight tests have demonstrated that this power reduction can be realized in practical flight. The agreement between theory and flight data is excellent. The application of a control system for the rear airplane leads to a considerable relief of the pilot and important power reductions could be achieved automatically by using this control system.

1. Introduction

It is well known that a number of migrating species of birds such as Swans, Geese and Cranes fly in regular V-shaped formations as shown in Fig. 1. The birds are located almost at the same flight level. They are ordered in swept lines and they keep so small spanwise distances that the wing tips of two adjoining individuals lie about one behind the other. Presently it is common understanding that this flight mode has two advantages: In these flight formations a power reduction takes place which leads to an aerodynamic benefit for all individuals. In addition in such regular formations exist good optical relations between the birds which lead to a communication benefit. Both aspects have been discussed recently by D. Hummel[1].

In the aeronautical sciences the problem of formation flight has been considered with respect to airplanes. C. Wieselsberger[2] was the first to give the correct explanation for the power reduction in such formations. After the development of aerodynamic theory, see e. g. H. Schlichting, E. Truckenbrodt[3], H. Schlichting[4] performed calculations on the drag reduction in symmetrical V-shaped flight formations of airplanes on the basis of Prandtl's lifting-line theory. Later P. B. S. Lissaman, C. A. Schollenberger[5] investigated optimum formation shapes and D. Hummel[6], [7], [8] extended the method of H. Schlichting[4] to arbitrarily shaped formations of wings having different span, weight and aspect ratio. More detailed

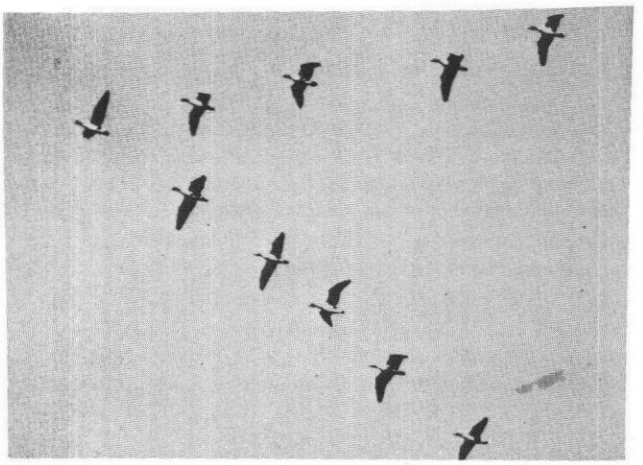

Fig. 1: Formation of migrating White-fronted Geese (Anser albifrons). Foto G. Rüppell, Braunschweig.

*) These investigations have been supported by Deutsche Forschungsgemeinschaft under contracts DFG Hu 254/5 and Hu 254/10.

investigations have been carried out by D. Hummel, K.-W. Bock[9] to include aileron deflections to compensate the rolling moment due to unsymmetric lift distribution. More recently formation flight has been studied theoretically on the basis of lifting-surface theory for unrolled, plane vortex sheets behind the wings by M. Beukenberg, D. Hummel[10] and for rolled-up vortex sheets by D. Hummel, M. Beukenberg[11]. All these theoretical investigations showed clearly that in formation flight considerable flight power reductions can be achieved. At least for two airplanes the benefit for the rear airplane lies in the order of magnitude of 15 %. Some principles of aerodynamic interference and theoretical results for flight formations will be discussed subsequently in section 3.

Further investigations concerning the practicability of formation flights of airplanes have been carried out at TU Braunschweig. For this purpose formation flights have been performed with two airplanes Dornier Do-28. The shape of the formation has been documented from a third airplane Do-27 and the energy consumption has been measured in flight. Results of these flight tests as well as comparisons with theoretical predictions will be shown in section 4.

During the flight tests the pilot of the rear airplane had difficulties to maintain simultaneously the proper flight condition and the correct location relative to the wake of the front airplane. To overcome these problems an automatic control system has been adopted for the rear airplane. The control process was based on an existing 3-axes digital autopilot, developed by A. Redeker[12],[13], which was initiated by a guiding system to optimize the power reduction. For this purpose the aileron deflection measured in flight was chosen to reach a maximum value. The control system has been tested under simulated conditions as well as in practical flight. The results will be discussed in section 5.

2. Notations

2.1 Symbols

$A = b^2/S$	Aspect ratio
b	Span
b'	Reduced span, Equ. (8)
c	Chord
$c_L = L/qS$	Lift coefficient
$c_D = D/qS$	Drag coefficient
e	Local relative power reduction, Equ. (4)
E	Total relative power reduction, equ. (7)
F	Thrust, throttle position
f	Upwash function, Equ. (10)
N	Flight power demand
$q = \rho V^2/2$	Dynamic pressure
$s = b/2$	Half span
S	Wing area
V	Flight speed
W	Weight
w	Upwash velocity, Equ. (1)
x, y, z	Rectangular coordinates, Fig. 2
$\Delta\xi = \Delta x/s$	
$\Delta\eta = \Delta y/s$	Dimensionless distances in
$\Delta\zeta = \Delta z/s$	flight formations, Fig. 2
α_w	Upwash angle, Equ. (1)
δ	Difference related to initial values
Γ	Circulation

2.2 Subscripts

c	Commanded quantity
ell	Elliptical circulation distribution
w	Pilot-controlled quantity
o	Single flight
1	Front airplane
2	Rear airplane
μ	Wing under consideration
ν	Inducing wing
$\overline{\ }$	Mean value over wing span (section 3) or over time (section 4)

Further notations may be taken from Section 3.1, Table 1 and the text.

3. Aerodynamics of formation flight

3.1 Basic ideas

The investigations following here are concerned with arbitrarily shaped flight formations of different wings μ in horizontal flight at the same level according to Fig. 2. It is assumed that the shape of the formation remains constant with respect to time. This means that all wings fly at

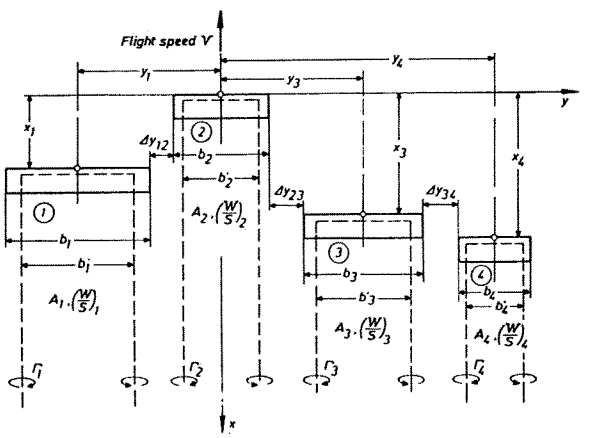

Fig. 2: Arrangement of wings in an arbitrarily shaped flight formation (example n = 4) and calculation of the interference effects by means of single horse-shoe vortices.

the same speed V. The corresponding dynamic pressure is $q = \rho V^2/2$. The different size of the wings is described by their span b_μ ($\mu = 1, 2, \ldots, n$) where n is the total number of wings present in the formation. If all wing spans are related to a reference span b, the corresponding dimensionless parameter is $B_\mu = b_\mu/b$. The planform shape is characterized by the aspect ratio $A_\mu = b_\mu^2/S_\mu$. For given values of A_μ and B_μ the wing area is $S_\mu/b^2 = B_\mu^2/A_\mu$. In the various positions μ of the formation the wing loading W_μ/S_μ may be different. According to the balance of the vertical forces the corresponding dimensionless parameter is the lift coefficient $c_{L\mu} = W_\mu/qS_\mu$ of each wing μ.

In horizontal flight of a single wing μ (subscript o) the lift $L_{o\mu}$ equals the weight W_μ and the power demand is $N_{o\mu} = D_{o\mu} \cdot V$, see Fig. 3. The drag consists of friction drag and of induced drag. The aerodynamic principle in flight formations is the fact, that each wing μ flies in an upwash field generated by all other wings ν of the formation. In general the upwash is a function $w_\mu(y_\mu)$ of the spanwise coordinate y_μ of the wing μ under consideration. Its average value over the wing span may be denoted as $\bar{w}_\mu$. Due to the upwash at each wing μ the flow direction and thus the direction of lift ($L_\mu = L_{o\mu}$) is turned at an upwash angle

$$\alpha_{w\mu} = \frac{\bar{w}_\mu}{V} \tag{1}$$

as indicated in Fig. 3. This leads to a drag reduction at the wing μ

$$\Delta D_\mu = L_\mu \cdot \frac{\bar{w}_\mu}{V} = L_{o\mu} \cdot \frac{\bar{w}_\mu}{V} \tag{2}$$

and the corresponding reduction in flight power demand is

$$\Delta N_\mu = \Delta D_\mu \cdot V = L_{o\mu} \cdot \bar{w}_\mu \, . \tag{3}$$

Based on the power demand for the same wing in single flight at the same speed V, the relative power reduction of wing μ is

$$e_\mu = \frac{\Delta N_\mu}{N_{o\mu}} = \frac{L_{o\mu} \cdot \bar{w}_\mu}{D_{o\mu} \cdot V} \, . \tag{4}$$

The total reduction of flight power demand of the whole formation of n wings is

$$\Delta N = \sum_{\mu=1}^{n} \Delta N_\mu \tag{5}$$

and based on the power demand of all wings μ in single flight

$$N_o = \sum_{\mu=1}^{n} N_{o\mu} \tag{6}$$

the relative power reduction of the whole formation can be expressed as

$$E = \frac{\Delta N}{N_o} \, . \tag{7}$$

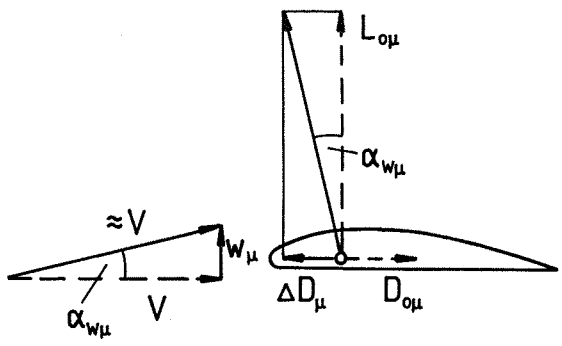

Fig. 3: Drag reduction ΔD_μ on wing μ due to upwash w_μ.

3.2 Calculation of the induced velocities

3.2.1 Horse-shoe vortex representation

The most simple analysis of flight formations can be achieved as follows. Each inducing wing ν is replaced according to Fig. 2 by a single horse-shoe vortex of span

$$b_\nu' = \frac{\pi}{4} b_\nu \tag{8}$$

and circulation

$$\Gamma_\nu = \frac{L_\nu}{\rho V b_\nu'} = \frac{2}{\pi} \frac{c_{L\nu}}{A_\nu} V b_\nu \, . \tag{9}$$

The induced upwash $w_{\mu\nu}$ at the wing μ generated by the horse-shoe vortex of wing ν is calculated from Biot-Savart's law as

$$\frac{w_{\mu\nu}(y_\mu)}{V} = \frac{c_{L\nu}}{\pi A_\nu} f_{\mu\nu}(y_\mu) \, . \tag{10}$$

This upwash distribution is a very good approximation for the values produced by a plane vortex sheet with an elliptic spanwise distribution of circulation. On the basis of Equ. (10) the mean value over the wing span can be calculated as

$$\frac{\bar{w}_{\mu\nu}}{V} = \frac{c_{L\nu}}{\pi A_\nu} \bar{f}_{\mu\nu} \tag{11}$$

with

$$\bar{f}_{\mu\nu} = \frac{1}{b_\mu} \int_{-b'_\mu/2}^{+b'_\mu/2} f_{\mu\nu}(y_\mu)\, dy_\mu \,. \qquad (12)$$

The upwash $\bar{w}_\mu$ at wing μ generated by all other wings ν of the formation is

$$\frac{\bar{w}_\mu}{V} = \sum_{\nu=1}^{n}{}' \frac{c_{L\nu}}{\pi A_\nu} \bar{f}_{\mu\nu} \qquad (13)$$

where $'$ denotes that the term for $\mu = \nu$ has to be omitted. The local and the total power reductions are then calculated from Equ. (4) and (7).

This simple theoretical analysis has been applied by H. Schlichting[4] as well as in various papers by D. Hummel[1], [6], [7], [8].

3.2.2 Unrolled vortex sheet representation

In the simple analysis of the interference problem for the induced upwash mean values over the wing span have been used. In this case the flow is symmetrical for each wing and no rolling moment occurs. To calculate the rolling moment due to unsymmetrical upwash distribution and to compensate it by means of proper aileron deflections a more detailed analysis is necessary. Fig. 4 shows a formation of n = 2 wings. Both wings and their wakes are replaced by a plane vortex sheet with bound vorticity on the wing and free vortices behind the wing. The free vortex sheet is assumed to be unrolled and to be located in the plane of the wing. For the calculation of the induced velocities different approaches are possible. D. Hummel, K.-W. Bock[9] used Prandtl's lifting-line theory[3] for the representation of the wings and the induced upwash in their vicinity has been calculated according to the method of K. Gersten[14]. In the calculations carried out by M. Beukenberg, D. Hummel[10] lifting-surface theory[3] has been applied and the induced velocities have been determined again by means of the method of K. Gersten[14]. Details may be taken from both original papers[9] and [10]. From both theories the rolling moment due to an unsymmetrical lift distribution against wing span turns out. For compensation some aileron deflections have been applied. This led for each wing to an unsymmetric lift distribution against span which produced no rolling moment. Although the corresponding load distribution turned out to be non-elliptic, a considerable power reduction turned out from this analysis, which was in the same order of magnitude as calculated by the more simple method discussed earlier. The calculation of the aerodynamic interference on the basis of a lifting-surface representation of the wing and for plane, unrolled free vortex sheets behind the wings has been extended by M. Beukenberg[15] to arbitrarily shaped formations of airplanes. In this method, the horizontal tails of the airplanes are also taken into account, pitching and rolling moments about the centre of gravity are balanced by proper deflections of the ailerons and the elevator and arbitrary locations of the airplanes including horizontal and vertical distances are possible.

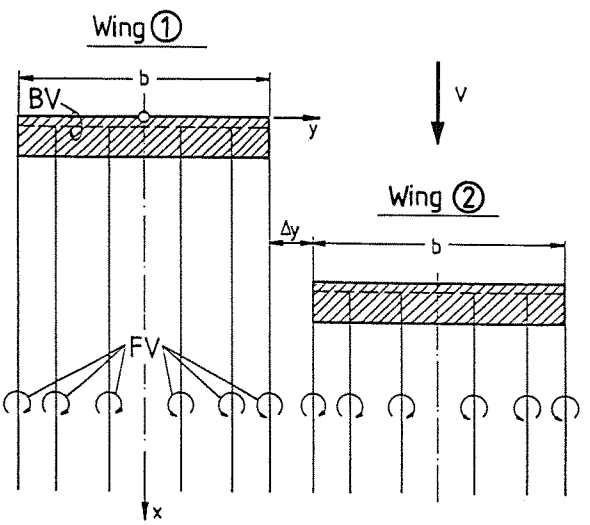

Fig. 4: Calculation of the interference effects by means of unrolled, plane vortex sheets, example n = 2 (BV bound vortex on the wing, FV free vortices behind the wing).

3.2.3 Rolled-up vortex sheet representation

A detailed analysis of flight formations of Geese by L. L. Gould, F. Heppner[16] shows some overlap of the wing tips. This means that in such formations according to Fig. 4 the spanwise distance is $\Delta y < 0$. Concerning the flight level observations by S. Schindler[17] showed that in flight formations of Cranes the leading individual flies at lowest level and the following birds are slightly staggered in height. Both details can be explained by the fact that the free vortex sheet behind a wing rolls up from both sides into two concentrated wing-tip vortices. Their distance is $b' < b$ as indicated in Fig. 2 and they are located above the plane of the wing. These details cannot be described by the unrolled vortex sheet representation according to Fig. 4. In the simple horse-shoe vortex representation according to Fig. 2, however, a certain overlap is possible up to a distance of $\Delta y = -s(4 - \pi)/4 < 0$. In this case the wing tip touches the free vortex of the adjacent wing. The details of the near wake behind the wing are not covered properly by this vortex model since the span b' according to equ. (8) is the asymptotic value related to elliptic load distribution [3] and the correct vertical location of the wing-tip vortex is not represented. If therefore optimum flight formations are considered and if details of the lateral and vertical distance of the wings are

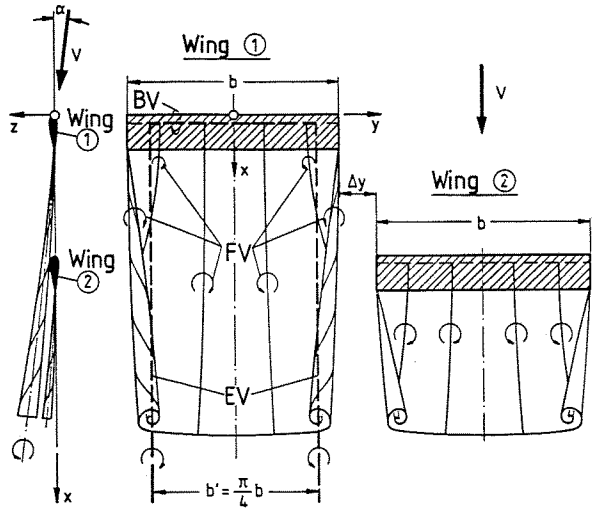

Fig. 5: Calculation of the interference effects by means of rolled-up vortex sheets, example n = 2 (BV bound vortex on the wing, FV free vortices behind the wing, EV equivalent single vortex, horse-shoe vortex).

discussed the rolled-up vortex sheet in the near wake has to be taken into account.

Fig. 5 shows a formation of n = 2 wings in which rolled-up trailing vortex sheets are considered. In calculations carried out by D. Hummel, M. Beukenberg[11] the lifting-surface theory of C. Urban, R. Behr, S. Wagner[18] has been used. In this method the shape of the wake turns out by means of an iteration procedure and the induced velocities generated by the non-planar vortex system are taken into account properly for the wing under consideration as well as for the evaluation of the mutual interference between the wings. Due to the iteration procedure calculations of this kind are extremely laborious. Some results are discussed subsequently.

3.3 Power reductions for wings

The power reduction in formation flight has been calculated according to different theoretical methods. Following here some typical results are shown in order to demonstrate the magnitude of the effects under consideration.

In the case of equal wings the problem reduces considerably. In the simple horse-shoe vortex analysis the aspect ratio A_μ has not to be specified and the span ratio is $B_\mu = 1$. From Equ. (4) and (13) yields

$$e_\mu = \left[\frac{c_{Di,ell}}{c_D} \right]_{o\mu} \sum_{\nu=1}^{n} \bar{f}_{\mu\nu} \qquad (14)$$

with

$$c_{Di,ell} = \frac{c_L^2}{\pi A} \,. \qquad (15)$$

Evaluations of Equ. (14) and (7) have been carried out for

$$(c_{Di,ell}/c_D)_{o\mu} = 0{,}5$$

which is the maximum range condition in single flight.

Fig. 6 shows the total power reduction E in flight formations of equal wings as a function of spanwise distance $\Delta\eta = \Delta y/s$ and of the number of wings n. It turns out that the power reduction increases considerably with decreasing spanwise distance of the wings. The power reduction increases also with increasing number of wings n but there exists a limiting curve for $n \to \infty$ which has already been given by H. Schlichting[4]. The result according to Fig. 6 is independent of the actual shape of the formation. This is the well-known displacement theorem of M. M. Munk[19]. Thus it turns out that all flight formations having the same lateral distances between the wings and the same number of wings achieve the same total flight power reduction. For small spanwise distances the total flight power reduction reaches remarkable values. Even for two wings (n = 2) total flight power reductions in the order of magnitude of 10 % are possible.

The distribution of the power reduction on the wings of the formation, however, depends strongly on the shape of the formation. Fig. 7 shows a typical example for formations of n = 15 equal wings at a spanwise distance $\Delta y = 0$. The wings are arranged on swept lines and the leading position n_1 is varied from $n_1 = 1$ (oblique line) over $n_1 = 4$ (unsymmetrical formation) to $n_1 = 8$ (symmetrical formation). The total power reduction E = 0.23 is the same for all these formations. In the leading position the power reduction is very low. This is due to the fact that the upwash decreases rapidly

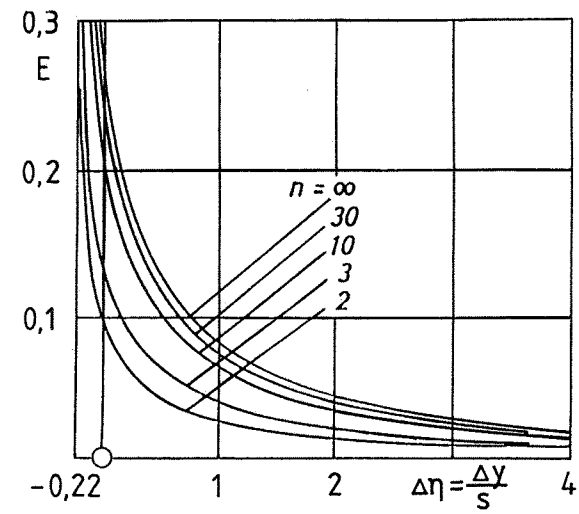

Fig. 6: Total power reduction in flight formations of equal wings as functions of spanwise distance and number of wings, $(c_{Di,ell}/c_D)_o = 0.5$.

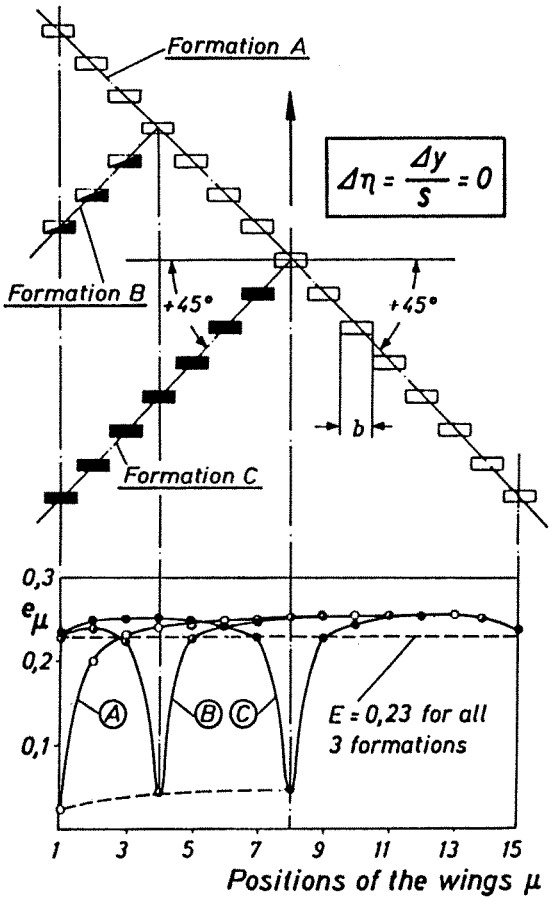

Fig. 7: Distribution of flight power reduction in 45° swept V-shaped formations of n = 15 equal wings at spanwise distance $\Delta y = 0$ and $(c_{Di,e}/c_D)_0 = 0.5$ for various leading positions n_1.
Formation A: Oblique line, $n_1 = 1$
Formation B: Unsymmetr. formation, $n_1 = 4$
Formation C: Symmetrical formation, $n_1 = 8$.

in upstream direction. The positions at both sides of the formation are also unfavourable since no neighbour-wings are present which would produce upwash. The worst position is those of the leading wing of a swept line formation ($n_1 = 1$) since both effects add. In the centre of straight lines the local power reduction lies over the average value.

If two wings are considered which fly side by side, the power reduction is equal for both wings. If one wing moves upstream the total power reduction for both wings remains constant according to Munk's theorem, but the front wing experiences a lower power reduction and the rear wing a larger one. In the limit of very large longitudinal distances the power reduction of the front wing tends to zero whereas the total power reduction, which is still present since a wake of the front wing exists, is concentrated on the rear wing. These results have been obtained on the basis of the simple horse-shoe vortex representation according to section 3.2.1. Further details may be taken from D. Hummel[6], [7], [8].

Improved calculations for flight formations have been carried out by D. Hummel, K.-W. Bock[9] in which Prandtl's lifting-line theory has been applied. The local spanwise distribution of the induced upwash $w_{\mu\nu}(y_\mu)$ rather than a mean value has been taken into account and the resulting rolling moment has been compensated by aileron deflections. It turned out that the improved analysis led to slightly larger values of the calculated power reduction, expecially for low spanwise distances. Results according to the simple horse-shoe vortex method may therefore be regarded as the minimum values of the power reduction which can be obtained.

Results for a more detailed analysis of the formation flight of two rectangular wings of aspect ratio A = 6, flying at a lift coefficient $c_L = 0.75$ and having a zero-lift drag coefficient $c_{D0} = 0.02$ are shown in Fig. 8. The longitudinal distance $\Delta\xi = \Delta x/s = 2$ is kept constant and the relative power reduction of the rear wing e_2 is plotted against the spanwise distance $\Delta\eta = \Delta y/s$. The dashed curve represents the results of the simple horse-shoe vortex method according to D. Hummel[1]. A certain overlap of the wing tips is possible and the adjacent free vortex is touched by the wing tip at $\Delta\eta = -0.22$. The results for a plane, unrolled vortex sheet representation by means of lifting surface theory including aileron deflections for rolling moment compensation according to M. Beukenberg, D. Hummel[10] are also shown for comparison. In this case an overlap of the wing tips cannot be described. As mentioned already the calculated power reduction is slightly larger than that given by the simple horse-shoe vortex method. In addition results of calculations with a rolled-up vortex sheet representation are shown. In this case the

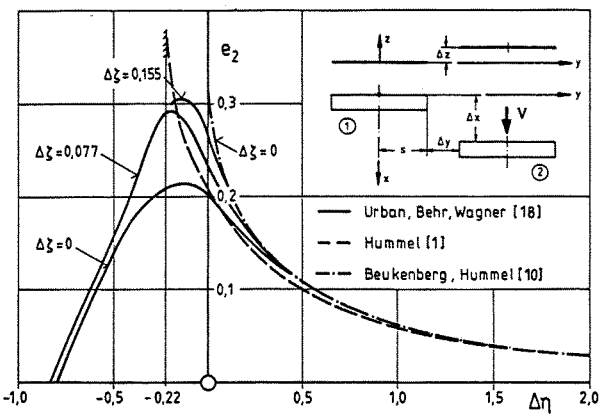

Fig. 8: Relative power reduction e_2 of the rear wing as function of the lateral distance $\Delta\eta = \Delta y/s$ for fixed longitudinal distance $\Delta\xi = \Delta x/s = 2$ and different vertical distances $\Delta\zeta = \Delta z/s$ for formations of two wings without and with overlaps of the wing tips. Comparison of the results according to different theories. (Wing parameters: aspect ratio $A_1 = A_2 = 6$, zero-lift drag coefficient $c_{D01} = c_{D02} = 0.02$, lift coefficients $c_{L1} = c_{L2} = 0.75$).

free vortex sheet is located above the plane of the wing. From both sides wing-tip vortices roll up and the effective span of the vortex wake behind the wing is smaller than the wing span. Aileron deflections have not been taken into account in these calculations. If both wings are located in the same plane, $\Delta\zeta = \Delta z/s = 0$, the power reduction, obtained for the rear wing, is considerably smaller than that calculated from lifting-surface theory with unrolled vortex sheets. This is due to the fact that the rear wing is now located below the region of maximum upwash. For strong overlap the rear wing passes below the vortex wake of the front wing continously into the region of downwash and a positive power reduction disappears at all. If the rear wing is slightly staggered in heigth relative to the front wing at $\Delta\zeta = 0.077$ the rear wing is still too low relative to the wake of the front wing, but the power reduction increases considerably, especially in the overlap region. For $\Delta\zeta = 0.155$ the rear wing is located aside the wing-tip vortex of the front wing and experiences maximum upwash. The power reduction too reaches a maximum for a certain small overlap. The comparison with the results according to lifting-surface theory with plane vortex sheet shows excellent agreement for $\Delta y > 0$. This means that calculations by means of the simpler theory are sufficient for positive spanwise distances, $\Delta y > 0$, whereas rolled-up vortex sheets have to be taken into account only for overlapping wing tips, $\Delta y < 0$. Further details may be taken from D. Hummel, M. Beukenberg[17].

3.4 Power reductions for airplanes

Comprehensive sample calculations for formations of two equal airplanes have been carried out for realistic flight conditions. For this purpose the following data were chosen

Wing:	Rectangular wing	$A_W = 6.0$
	Ailerons at wing tip	$\eta_Q = y_Q/b = 0.66$, $\lambda_K = c_K/c = 0.25$
Horizontal tail:	Rectangular tail	$A_T = 3.0$
	Size	$b_T/b_W = 0.45$
	Position	$\Delta\xi_T = \Delta x_T/s = 0.9$, $\Delta\zeta_T = \Delta z_T/s = 0.1$
	Elevator: Free floating tail	
Vertical tail:	Aspect ratio	$A_V = 1.5$
	Taper ratio	$\lambda_V = 0.5$
	Leading-edge sweep	$\varphi_V = 24°$
	Size	$b_V/b = 0.15$
	Rudder	$c_K/c_i = 0.3$
	Position	$\Delta\xi_V = \Delta x_V/s = 0.8$, $\Delta\zeta_V = \Delta z_V/s = 0$
Centre of gravity position		$x_{CG}/c = 0.25$
Zero-lift drag coefficient		$c_{Do} = 0.05$

Wings and tails in the formation have been taken into account by lifting-surface theory and plane vortex sheets. For each airplane the pitching moment about the centre of gravity was balanced by means of elevator deflections of the whole horizontal tail and the rolling moments due to unsymmetrical spanwise load distribution were compensated by means of aileron deflections. The resulting yawing moment again was balanced by corresponding deflections of the rudder of the vertical tail. More details about the geometry of the flight formations as well as on the calculation procedure may be taken from M. Beukenberg, D. Hummel[10] and M. Beukenberg[14].

The power reductions achieved in this flight formation at a constant lift coefficient $c_{L1} = c_{L2} = 0.7$ are shown in Fig. 9 as functions of the spanwise distance $\Delta\eta = \Delta y/s$ for a fixed longitudinal distance $\Delta\xi = \Delta x/s = 2$ and a fixed vertical distance $\Delta\zeta = \Delta z/s = 0$. The total power reduction for both airplanes is quite remarkable. For flight wing tip behind wing tip a total reduction of about

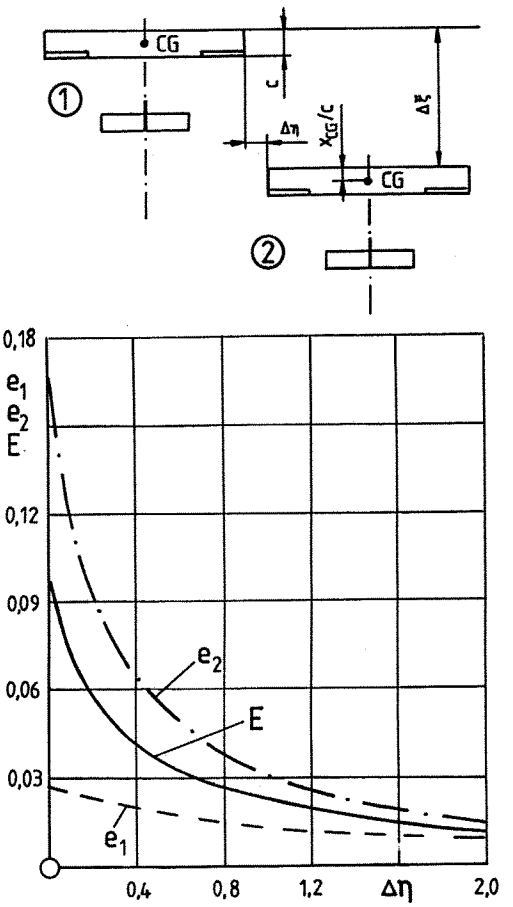

Fig. 9: Relative power reductions E, e_1, e_2 as functions of the lateral distance $\Delta\eta = \Delta y/s$ for fixed longitudinal distance $\Delta\xi = \Delta x/s = 2$ and fixed vertical distance $\Delta\zeta = \Delta z/s = 0$ for formations of two sample airplanes (Flight parameters: Lift coefficients $c_{L1} = c_{L2} = 0.7$, zero-lift drag coefficients $c_{Do1} = c_{Do2} = 0.05$, centre of gravity position $x_{CG}/c = 0.25$).

10 % is achieved. Due to the longitudinal distance of both airplanes the power reduction is lower for the front airplane and higher for the rear airplane, reaching about 17 % for flight with wing tip behind wing tip, $\Delta\eta = 0$.

The corresponding aileron deflections are shown in Fig. 10. They are opposite in sign for both airplanes and they are equal in size for flight side by side, $\Delta\xi = 0$, which is shown for comparison. For decreasing spanwise distance the aileron deflections increase. In the case of a longitudinal distance of both airplanes the aileron deflections are small for the front airplane and large for the rear airplane. The same applies in principle for the deflections of the rudder of the vertical tail, but the deflection angles are smaller; see M. Beukenberg[14].

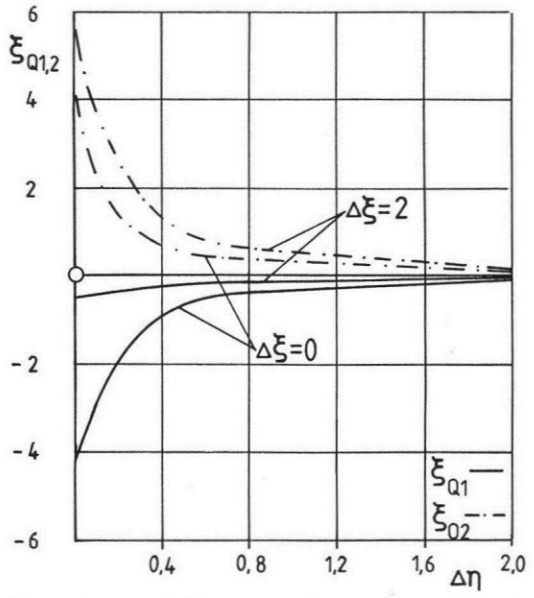

Fig. 10: Aileron deflections ξ_{Q1}, ξ_{Q2} as functions of the lateral distance $\Delta\eta = \Delta y/s$ for fixed longitudinal distance $\Delta\xi = \Delta x/s = 2$ and fixed vertical distance $\Delta\zeta = \Delta z/s = 0$ for formations of two sample airplanes. (Flight data as in Fig. 9).

Aileron deflection angles can be measured easily in flight. They can be used as a measure for the proper position of the rear airplane with respect to the wake of the front airplane. In an optimum flight formation the aileron deflections reach a maximum and this maximum can be used to find the proper positions.

4. Measurements of the power reduction in flight

4.1 Flight tests

Formation flights of two airplanes have been carried out in order to find out whether the large power reductions predicted by methods of theoretical aerodynamics can be realized in practical flight conditions. For this purpose two research aircraft Dornier Do 28-D1 of Deutsche Forschungsanstalt für Luft- und Raumfahrt, Forschungszentrum Braunschweig, DLR (identification D-IFZB) and of Technische Universität Braunschweig (identification D-IBSW) were available. For the photographic documentation of the positions of the two aircraft relative to each other in formation flight a third aircraft Do 27 of DLR (identification D-EDFL) has been used.

The front airplane (D-IFZB) flew at constant flight level with constant velocity and acted as a "vortex generator" for the rear airplane, see Fig. 11. In addition the front airplane was equipped with a device which enabled the rear airplane to find the proper position. For this purpose a small (diameter 20 cm, height 40 cm) and light cone was carried along by means of a thin wire of variable length which could be adjusted to mark the longitudinal distance to be adopted by the rear airplane. In the correct longitudinal position the cone was located aside the rear airplane, and the cone could also be used to find the proper vertical position. For a certain period of time the rear airplane kept a constant position relative to the front airplane, and in this time its data aquisition system measured all quantities which are necessary for the evaluation of its flight state. During the measuring time photos of the formation were taken from the third accompanying aircraft Do 27 (D-EDFL) in order to be able to determine the actual positions of both aircraft by a quantitative evaluation. A photo of this kind is shown in Fig. 11. The position of the cone is marked by a circle and the numbers indicate the time for a proper correlation between data aquisition and position.

During the flight tests the following technique was used. For given longitudinal distance a large lateral distance was used first to adjust the velocities of the two airplanes and this state was used as the reference state without interference.

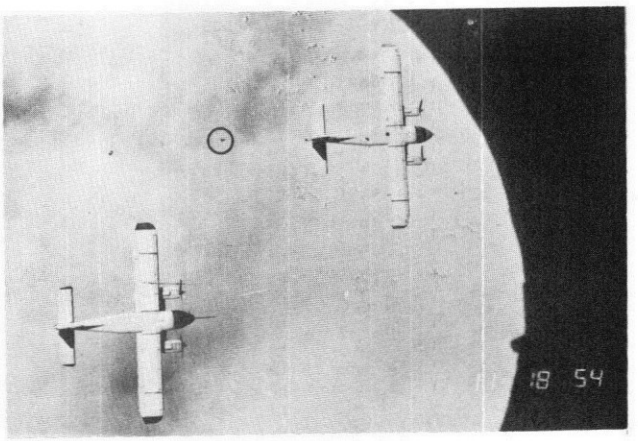

Fig. 11: Formation flight of two airplanes Do-28 at longitudinal distance $\Delta\xi = \Delta x/s = 4$ and lateral distance $\Delta\eta = \Delta y/s = 0$. (Circle indicates cone position).

The lateral distance was then reduced to find a position with large interference effects. The wing tip behind wing tip position was adopted using some radio guidance from the third airplane. Concerning the vertical position the level of the wing tip vortices had to be found. For this purpose maximum interference effects were used. The flight level of the rear airplane was adjusted in such a way that the throttle position for constant flight speed became a minimum and the aileron deflections reached a maximum. The corresponding position was kept for some minutes to collect the data and to document the positions. The lateral distance was then increased in steps and finally the reference position without interference effects was repeated. This technique was applied for various longitudinal distances. In addition the flight tests have been carried out for two different flight speeds V = 80 kts. and V = 100 kts. in order to vary also the lift coefficient.

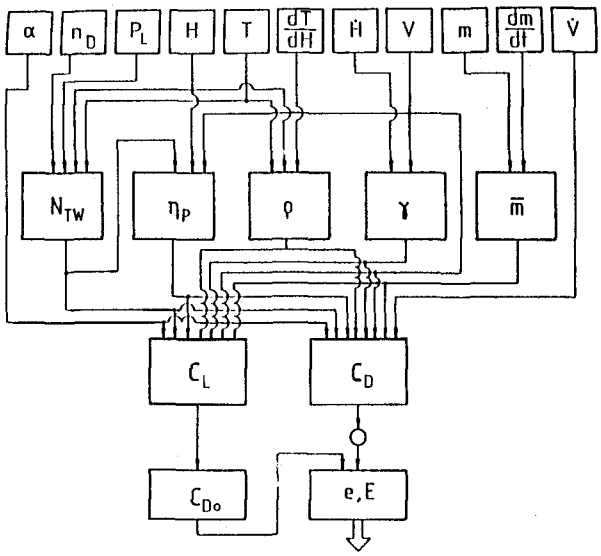

Fig. 12: Scheme for the evaluation of the flight test data.

4.2 Data acquisition and corrections

All measuring quantities which have been registered in flight are shown in Tab. 1. For the evaluation periods of time with roughly constant data have been chosen and the data from these periods have been used as mean values with respect to time. The evaluation scheme is shown in Fig. 12. The directly measured quantities are collected in the first line. The temperature gradient with respect to the altitude, dT/dH, has been determined from the flight data during climb and descend. A weight analysis of the aircraft led to the mass of the airplane and the mass gradient with respect to time has been deduced from the fuel consumption of the aircraft in flight. The quantities in the second line have been determined from the directly measured data. The engine power N_{TW} and the propeller efficiency η_P resulted from the characteristic diagrams of the engine and the propeller, which are both known. The density of the air ρ has been calculated for the measured temperature distribution as function of the altitude by means of a polytropic athmosphere model. The flight path inclination angle γ has been evaluated using the vertical and the total flight velocity. The aircraft mass $\bar{m}$ which is present for a measuring period has been determined by means of the take-off mass of the aircraft, the mass gradient dm/dt and the time interval between take-off and the middle of the measuring period.

Table 1: Flight test data

I)	Data necessary for the determination of the power reduction	
	Engine rotation rate	n_D
	Intake pressure	p_L
	Altitude	H
	Temperature	T
	Rate of climb	dH/dt
	Speed	V
	Angle of attack	α
	Time	t
II)	Data necessary for the determination of the flight regime	
	Horizontal acceleration	dV/dt
	Aileron deflection	ξ_Q
	Rudder deflection	ζ_S
	Elevator deflection	η_H
	Pitch attitude	Θ
	Angle of sideslip	β
	Angle of bank	φ
	Roll rate	p
	Pitch rate	q
	Yaw rate	r

For the determination of lift and drag coefficient it is assumed that the flight path of the aircraft is located in a vertical plane and that the velocity vector lies in the plane of symmetry of the aircraft. In this case simple equations of motion can be used and for lift and drag coefficient yields

$$c_L = \frac{2\,\bar{m}g}{\rho V^2 S}\cos\gamma - \frac{N_{TW}\cdot\eta_P}{\rho V^3 S}\sin(\alpha + i_p) \qquad (16)$$

$$c_D = \frac{N_{TW}\cdot\eta_P}{\rho V^3 S}\cos(\alpha + i_p) - \frac{2\,\bar{m}g}{\rho V^2 S}\sin\gamma - \frac{2\bar{m}}{\rho V^2 S}\frac{dV}{dt}\,. \qquad (17)$$

In these equations $\alpha + i_p$ is the angle between the free stream direction and the engine axis and S is the wing reference area. All quantities in Equ. (16) and (17) are available in order to evaluate c_L and c_D. Equ. (16) and (17) have also been applied for flight conditions with large spanwise distances

between the two aircraft. This led to data for the reference case without interference, and since a reliable polar diagram for the aircraft Do-28 was available, from these data the zero-lift drag coefficient of the aircraft in single flight, c_{Do}, could be determined. The relative power reduction according to equ. (4) has been finally calculated for the rear airplane 2 from

$$e_2 = \frac{\Delta N_2}{N_o} = 1 - \frac{N_2}{N_o} = 1 - \frac{c_{D2}}{c_{Do}} , \qquad (18)$$

where c_{D2} denotes the drag coefficient in formation flight.

The Equ. (16), (17) and (18) are only valid for symmetrical flow. Results of the inflight tests showed, that some small angles of sideslip were present. Therefore the drag coefficients evaluated from Equ. (17) as well as the aileron and rudder deflections include some contributions from the unsymmetrical flow. A correction had to be carried out to compensate this effect and to obtain results which are due to the interference effect only.

Hence the drag coefficient and the aileron and rudder deflections were measured in flight tests with a single DORNIER DO-28 research aircraft as function of the angle of sideslip. During these flight tests the lift coefficient was kept constant. The corrections for the drag coefficient have been determined as

$$\Delta c_D(\beta) = c_D(\beta) - c_D(\beta = 0) \qquad (19)$$

and for the aileron and rudder deflections as

$$\Delta \xi_Q(\beta) = \xi_Q(\beta) - \xi_Q(\beta = 0) \qquad (20)$$

$$\Delta \zeta_S(\beta) = \zeta_S(\beta) - \zeta_S(\beta = 0) . \qquad (21)$$

All results discussed in section 4.3 include these corrections.

4.3 Results and comparison with theory

As a result from Equ. (18) the power reduction is obtained as the difference of two small drags, measured in flight. This can be done successfully, if the drag in single flight and the drag in formation flight are measured by the same procedure. For this reason, the drag characteristic in single flight was also measured during the formation flight tests and the measured characteristic for the aircraft DO-28 turned out in excellent agreement with the drag characteristic obtained by M. Beukenberg [15] and A. Redeker [12], [13]. Fig. 13 shows the relative power reduction of the rear airplane, e_2, in formations of two equal airplanes DO-28 as function of the lateral distance $\Delta\eta$ for different longitudinal distances $\Delta\xi$.

For the lateral distance $\Delta\eta = 0$ a considerable power reduction e_2 of about 15 % was obtained from the formation flight tests. With increasing lateral distance, the measured relative power reduction e_2 decreases rapidly. Included in Fig. 13 is the theoretical curve for a longitudinal distance $\Delta\xi = 4$. Due to the fact, that there is only a minor change in power reduction for longitudinal distances in the order of magnitude of $\Delta\xi = 4$ or more, it is worthwhile to compare all the measured values with this theoretical curve. Excellent agreement between theory and experiment for the relative power reduction e_2 as function of the lateral distance $\Delta\eta$ turns out.

A similar result is obtained for the aileron deflections of the rear airplane, plotted in Fig. 14 as function of the lateral distance $\Delta\eta$. The theoretical curve is included for the longitudinal distance $\Delta\xi = 4$. The aileron deflections decrease rapidly with increasing lateral distance, as mentioned earlier for the relative power reduction. The comparison of Fig. 13 and 14 shows evidently that the measured aileron deflections are a very sensitive criterion for the achieved power reduction.

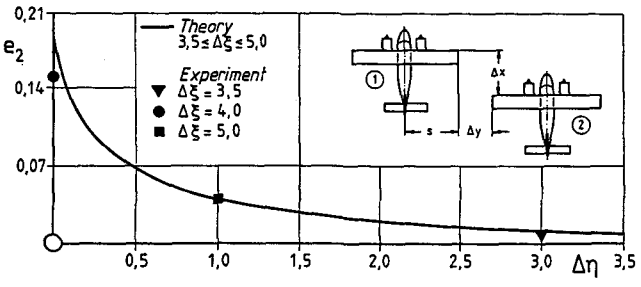

Fig. 13: Relative power reduction e_2 of the rear airplane as function of the lateral distance $\Delta\eta = \Delta y/s$ for different longitudinal distances $\Delta\xi = \Delta x/s$ for formations of two airplanes DO-28. Comparison between theory for $\Delta\xi = 4$ and experiment. (Flight parameters: $c_{L1} = 0.84$, $c_{L2} = 0.93$, $c_{Do1} = c_{Do2} = 0.0489$).

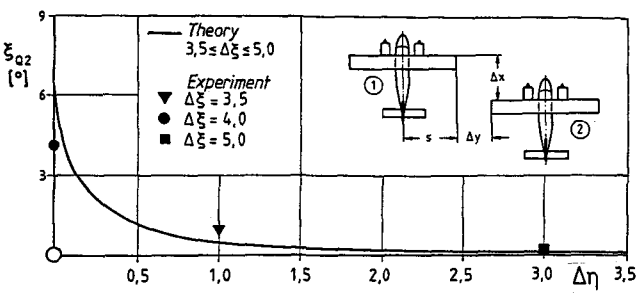

Fig. 14: Aileron deflections at the rear airplane as function of the lateral distance $\Delta\eta = \Delta y/s$ for constant longitudinal distance $\Delta\xi = 4$. Comparison between theory and experiment for two airplanes DO-28. (Flight parameters: $c_{L1} = 0.84$, $c_{L2} = 0.93$, $c_{Do1} = c_{Do2} = 0.0489$).

Similar results have been obtained for higher lift coefficients and larger longitudinal distances. But in these cases the results yield larger differences between theory and experiment. These differences increase for higher lift coefficients c_L and larger longitudinal distances $\Delta\xi$. These differences are due to the fact that the pilot of the rear airplane had some difficulties to maintain simultaneously the proper flight condition and the correct location relative to the wake of the front airplane. To overcome these problems an automatic control system has been designed in order to be able to carry out formation flights by means of an autopilot. The basic ideas of the realisation of this control system and the main results are discussed in the subsequent section.

5. Automatic control of formation flights

5.1 Basic ideas

The optimum position of the rear airplane relative to the front airplane in lateral and longitudinal direction is defined by the maximum power reduction achieved by the rear airplane. Hence an autopilot for formation flight has to solve the problem to find and keep this optimum position for some time. In more detail it is necessary to search for the proper position of the rear airplane relative to the wake of the front airplane. This wake induces upwash velocities in its vicinity. If the rear airplane flies close to this wake, it achieves a power reduction which is especially high, if the induced upwash velocities are large. The optimum position in a flight formation is therefore characterized by a maximum induced upwash velocity along the wing span of the rear aircraft. Hence the optimum power reduction can be replaced by the maximum induced upwash velocity along the wing span, when searching for the optimum position.

Taking into account all the informations about the wake of an aircraft and the known behaviour of an aircraft flying close to such a wake as well as the available sensor equipment of the experimental airplane, explained in detail by A. Redeker [13], it is possible to realize an autopilot solving the problem discussed above without big changes of the aircraft's equipment. For this purpose the decision was made to use an adaptive extremum controller. Such a technique means, that the aircraft has to perform always a motion to stay in the vicinity of the maximum power reduction. This means, that there is a loss in power reduction, compared to a stationary flight at the optimum. On the other hand the necessary technical expense is very small. The elements of the autopilot for formation flights are discussed in some detail in the following section.

5.2 Elements of the control system

5.2.1 Flight controller for the longitudinal motion

The autopilot for formation flight is based on a controller for the longitudinal motion of the used research aircraft DO-28 developed by A. Redeker [12], [13]. This is a modern structured flight controller with state feedback, able to work on a large number of disturbance variables and command inputs. This is possible due to the application of a quasi-stationary, non linear state model of the aircraft motion, which has the same order as the controlled system itself. Beside the pilot controlled actuator-variables, the model contains also the commanded states of the controlled system. Now it is possible to compare actual and commanded states on the level of the states of the controlled system and model. The structure of this controller for the longitudinal part of the aircraft motion together with all in- and output variables shows Fig. 15.

Such a controller is able to work in different modes. The most important modes for formation flight applications are Altitude Hold and Altitude Acquire. The air speed is kept constant automati-

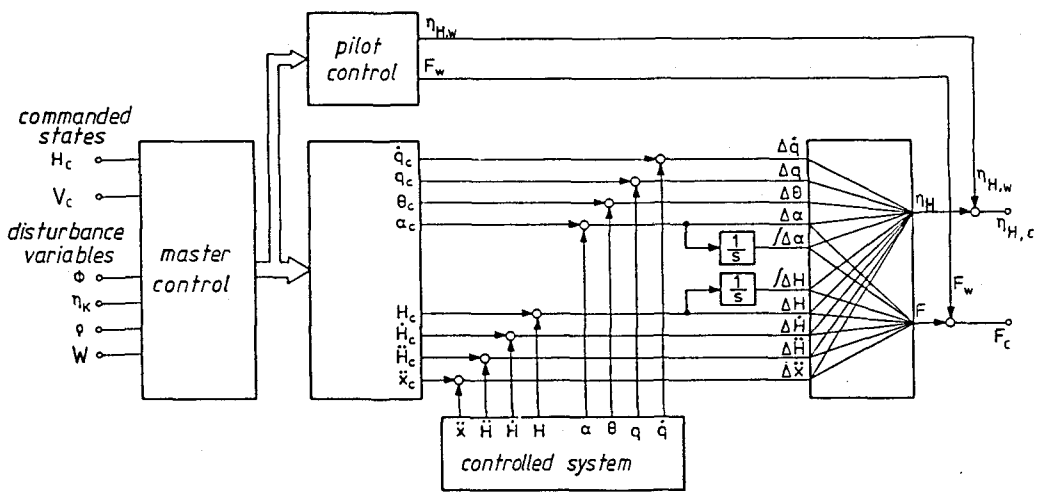

Fig. 15: Structure of the longitudinal part of the experimental flight controller, including all in- and outputs.

cally in both modes. It is possible to change the modes in flight directly.

In the mode Altitude Hold a commanded reference altitude can be kept constant together with the commanded true air speed. This is possible, although some external disturbances are present, e.g. bank angles, turbulence or changes of the flap position.

The mode Altitude Acquire controls the transition from one flight level to another. The rates of climb or descent can be commanded up to the maximum possible values. Again the commanded true air speed is kept constant.

5.2.2 Flight controller for the lateral motion

Supplementary to the flight controller for the longitudinal motion a corresponding controller for the lateral motion was added. The basic functions of this controller are yaw- and rolldamping. Beside these basic functions, the controller can hold a commanded heading or a commanded position line. This new part of the flight controller is realized also as state feedback controller. By controlling the position line indirect pilot control together with an inverse model of the controlled system is used. The structure of this controller for the lateral motion is shown in Fig. 16.

Beside Heading Hold additional Position Line controlling is essential for formation flight. To keep the distances in lateral direction during formation flights a very high accuracy in following a certain position line is necessary. Thereby the position line is generated artifically. When the controller is activated, a coordinate-system is created, the x-axis of which is equal to the actual heading. Now the lateral deviation from the commanded position line can be calculated as

$$\Delta y = \int_0^\infty V \cos(\alpha - \Theta)(\psi - \psi_c)dt \ , \qquad (22)$$

where $\psi - \psi_c$ is the difference between actual and commanded heading. Equ. (22) is exactly valid, if the angle of sideslip is zero. As long as the flight controller for the lateral motion contains a yaw-damper, this assumption is fulfilled.

5.2.3 Extremum controller for formation flight

The two controllers for the longitudinal and lateral motion of the aircraft are the base for the formation flight controller. As stated by H.G. Jacob [20] extremum controllers are adaptive controllers, which control the actuators of a system in such a way, that the cost criterion of the system stays at its maximum. This is normally possible, although unknown external disturbances and changes of the nonlinear system characteristics take place. The principle structure of such a system adapted to the application of formation flight is shown in Fig. 17.

In contrary to ordinary control systems, which compensate the deviation between the control variables and the commanded values in the presence of unknown external disturbances, an extremum controller keeps the criterion of cost effectiveness at a maximum. Such a process can only be used, if there exists between the control variables and the system characteristics a nonlinear dependence with an extremum.

From the nonlinear characteristics and the existence of an extremum follows, that the value of the criterion of cost effectiveness has to be known at least at two points of the performance characteristic. In this case the direction of the maximum is obtainable. Due to a decision criterion magnitude and direction of the next step towards the maximum can be calculated and performed. Now the value of the cost criterion is determined for the new point of the performance characteristic and the next loop can be started. It is evident, that such a procedure comes never to rest, because it searches always for the maximum. Therefore such systems can never stay at the maximum, but they are normally close to it. Due to this motion a loss exists, compared to a control system operating at the optimum. In addition, due to this motion the system is able to compensate unknown influences on the value of the cost effectiveness.

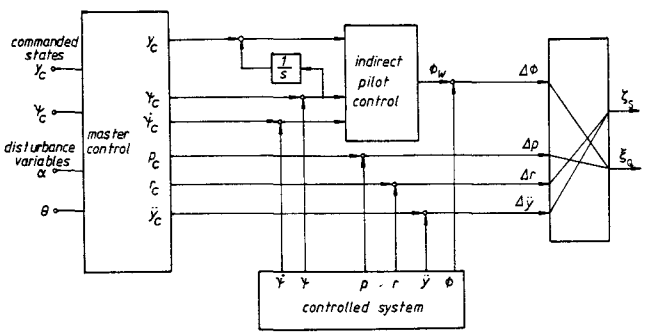

Fig. 16: Structure of the lateral part of the experimental flight controller, including all in- and outputs.

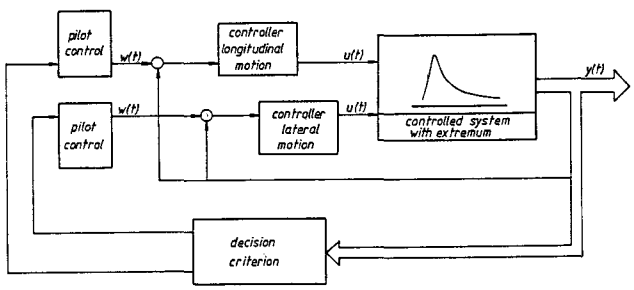

Fig. 17: Structure of the flight controller for formation flights, designed as extremum controller (u(t) control variables, w(t) pilot-controlled variables, y(t) output variables).

In formation flight the induced upwash velocity or the power reduction as function of the rear aircraft's position in lateral direction relative to the wake of the front aircraft can be used as the cost effectiveness. Thereby the assumption is made, that the distance in flight direction and the air speed are kept constant.

The motion is initiated by a new commanded flight level or position line. From the measured values of the induced upwash velocity and the aileron deflection at the actual position, a new position is calculated by means of the decision criterion, which compares those measured values at the old position with that measured at the actual position. Then the controller for the longitudinal and lateral motion guides the airplane into that new position. This procedure is repeated again and again.

5.2.4 The decision criterion

An important part of any extremum process is the decision criterion. This criterion allows the determination of the direction towards the maximum of cost effectiveness from system informations at several points of the performance characteristic. At any point during the flight mean values of the air speed, manifold pressure, altitude, position line deviation, upwash velocity and aileron deflection are measured. The corresponding upwash velocity is used as criterion of cost effectiveness, because of its proportionality to the power reduction under the assumption, that the air speed is constant and the performance is proportional to the thrust. In formation flight the upwash velocity as function of the lateral distance shows a defined maximum. Therefore the upwash velocity can be used as a criterion for the cost effectiveness.

With reference to H.G. Jacob[20] the criterion for the motion in vertical direction is

$$\Delta H = A(1-B\alpha_w)\,\mathrm{sign}[(H_n-H_{n-1})(\alpha_{w,n}-\alpha_{w,n-1})]. \quad (23)$$

A is the maximum vertical step size towards the extremum, B is a constant which controls the effect of the upwash on the step size and n, n-1 denote two subsequent positions. The step size decreases when the extremum is approached. On the other hand the step size is large, if a downwash velocity is detected. The last factor influences the direction of motion. As long as the upwash increases this direction is held. But if the upwash decreases, $\alpha_{w,n} - \alpha_{w,n-1} < 0$, the direction of motion is changed. This procedure holds the process in the vicinity of the optimum.

The strategy for the motion in horizontal direction is very similar. It is important to notice, that the aircraft has large dimensions in lateral direction, but the upwash velocity is measured only in the plane of symmetry, depending on the available measuring equipment, see A.Redeker [13] and P.Vörsmann [24]. Hence the maximum upwash is detected, when large parts of the half-wing, next to the wake of the front airplane, are already in the downwash region of the wake. This can be avoided, if the aileron deflections are used instead. It is evident from Fig. 13 and 14, that the aileron deflection is proportional to the achieved power reduction or upwash along the wing span. This means, that aileron deflections are an excellent sensor for the induced upwash velocity. Now the criterion for the lateral motion is given by

$$\Delta y = C(1-D\xi_Q)\,\mathrm{sign}[(y_n-y_{n-1})(\xi_{Q,n}-\xi_{Qn-1})] \quad . \quad (24)$$

This criterion has the same structure as that for the vertical motion. Both decision criterions are characterized by little calculational effort and fast compensation of disturbances as well as by a reliable guidance of the motion towards the maximum of cost effectiveness.

5.3 Behaviour of the control system in simulation tests

The theoretical investigations of the aircraft motion in a flight formation were based on the linearized differential equations of motion. The flight controller for formation flights, explained in section 5.2, was integrated completely in the simulation procedure. The wake of the front airplane was simulated by a horse-shoe vortex. The viscous core was taken into account in order to overcome the problem of infinite induced velocities. Based upon the exact solution of the Navier-Stokes-equations for a two-dimensional vortex-filament, the induced upwash velocity of the horse-shoe vortex system can be calculated according to W.Kaufmann [21] and K. Kirde [22]. Details of this simulation may be taken from M. Beukenberg [15].

5.3.1 Longitudinal motion

Fig. 18 shows the behaviour of the formation flight controller for the longitudinal motion. The variables plotted with respect to time are: distance in longitudinal direction δx and distance in vertical direction δz from the initial position, induced downwash velocity $-\delta w$, pitch angle $\delta\Theta$, thrust variation δF and elevator position angle $\delta\eta_H$. At the initial position, the rear aircraft is located five wing spans ($\Delta x/b=5$) behind and one wing span ($\Delta z/b=1$) below the front aircraft and the lateral distance is $\Delta y/b=0$. This means that the wing tip of the rear airplane is located next to the wake of the front aircraft.

Starting from this position, the controller should guide the aircraft into a position relative to the wake with large power reduction. The motions of the aircraft commanded by the controller are clearly visible, e.g. by the variation of the vertical position. The relative quick sequence of the commanded steps create the slightly rough outcome. It is clearly indicated, that the controller leads the rear aircraft within three steps into a favourable position relative to the wake of the front aircraft. Due to the continuous sequence

of steps this favourable position can not be fixed. The process shows more or less large deviations from the optimum position. Favourable positions are characterized by a large induced upwash velocity together with a small throttle position δF.

As an example, the time interval between 135 < t < 170 s is chosen. The mean vertical position δz = -15.39 m shows only a small deviation from the optimum value δz = -15m. Hence the rear aircraft achieves an upwash velocity of w = 0.726 m/s and a 14.3 % smaller throttle position. Mean values calculated over the whole simulation interval are for the vertical position δz = -16.05 m, the induced upwash w = 0.468 m/s and the throttle position -8 %. Nevertheless there is a remarkable power reduction. The search motion leads only to a small deviation in the longitudinal position δx which is not larger than ±1.0 m.

5.3.2. Lateral Motion

The behaviour of the extremum controller was also simulated for the lateral motion. At the initial position the rear aircraft was located five wing spans behind ($\Delta x/b=5$) the front aircraft at the same altitude. The lateral distance was slightly larger than one wing span ($\Delta y/b=1,3$). Fig. 19 shows

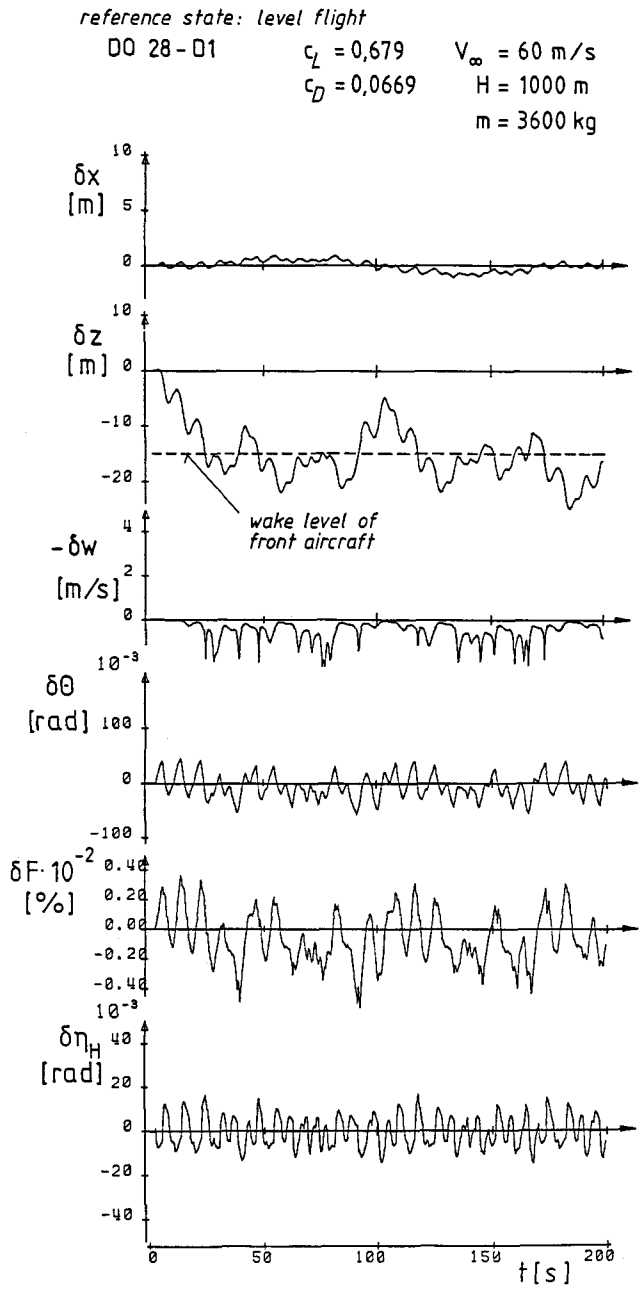

Fig. 18: Behaviour of the longitudinal part of the flight controller in formation flight. Results of simulation tests.

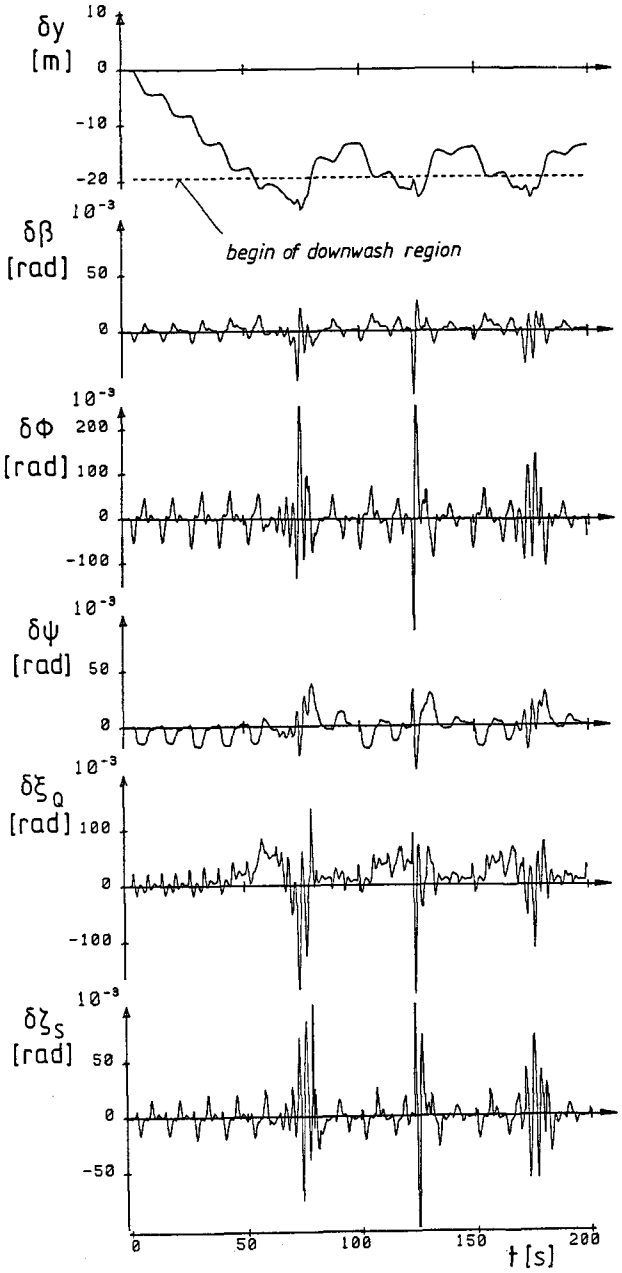

Fig. 19: Behaviour of the lateral part of the flight controller in formation flight. Results of simulation tests.

the results of the simulation by the plotted variables for lateral position δy, angle of yaw $\delta\beta$, bank angle $\delta\Phi$, heading $\delta\Psi$, aileron deflection $\delta\xi_Q$ and rudder deflection $\delta\zeta_S$. The optimum lateral position is included in Fig. 19 as dashed line in the diagram for the lateral position.

The approach of the rear airplane to the wake of the front airplane can be seen clearly by the change of the variables due to the commanded position changes. With decreasing distance from the wake in lateral direction the aileron deflection increases. This deflection is necessary to compensate the resulting rolling moment due to the nonuniform distribution of the induced upwash along the wing span. The size of the aileron deflection is in excellent agreement with the values calculated from the theory in section 3.

After four cycles, the phase of approach has finished, because the rear airplane has reached a lateral position close to the wake. From now on, the formation flight controller holds the rear aircraft in a nearby position relative to the wake of the front airplane. Thereby it can happen, that the rear aircraft moves partially into the downwash region of the wake of the front airplane. The result is a very unhomogeneous upwash distribution along wing span. In this case small variations of the lateral position produce significant changes of rolling and yawing moment. These are the reasons for the strong variations of the aircraft's state and of the actuators in Fig. 19. But the formation flight controller is able to stabilize this situation, which is characterized by strong interference effects. Indeed a high activity of the actuators is observed. The controller keeps the rear aircraft close to the wake of the front airplane and the deviations in lateral distance are within a semi wing span.

Although the controller meets very strong interference effects in the lateral motion, the rear aircraft is held in a favourable position relative to the front airplane. The quality of the achieved position changes only slightly with the occurrence of turbulence or changes in the heading of the front airplane.

5.4. Behaviour of the control system in flight tests

The controller was installed in the research aircraft DO-28 and tested in formation flight. Again the flight tests have been carried out in cooperation between TU Braunschweig and Deutsche Forschungs- und Versuchsanstalt für Luft- und Raumfahrt (DLR), Forschungszentrum Braunschweig. An airplane of type DORNIER DO-228 of DLR (identification D-CODE) was available and acted as "vortex generator". The research aircraft DORNIER DO-28 of Technische Universität Braunschweig (identification D-IBSW) completed the formation. For the photographic documentation of the positions of the two aircrafts relative to each other in formation flight, a third aircraft DO-27 of DLR (identification D-EDFL) was available.

5.4.1 Behaviour in single flight

First of all the longitudinal part of the controller for formation flights was tested. Fig. 20 shows a typical result. It is evident, that the controller keeps the air speed constant. This is important for formation flights because the longitudinal distance is kept constant by holding the air speed. But even more important is the vertical position. Fig. 20 shows the commanded altitude as dashed line. The altitude steps commanded by the controller are clearly visible. The deviations of the flight altitude (full line) from the commanded altitude are within 2.5m, which can be regarded as satisfactory. The climb rate shows also good agreement with the commanded values. The manifold

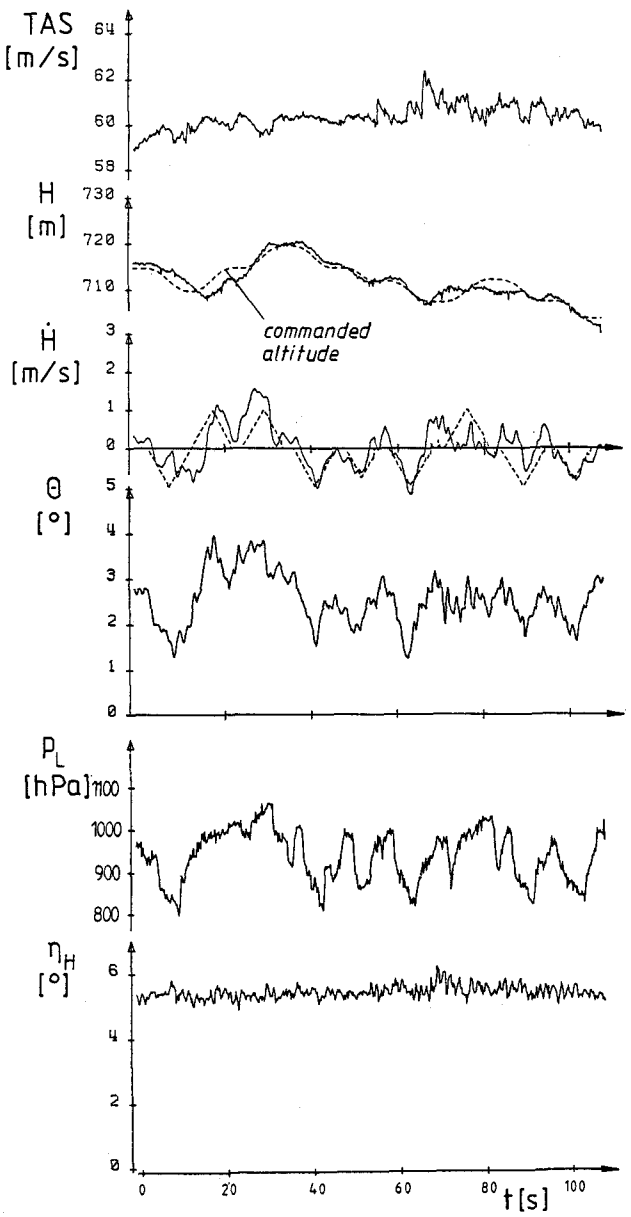

Fig. 20: Behaviour of the longitudinal part of the flight controller in single flight during flight tests of an airplane DO-28.

pressure p_L reflects clearly the necessary thrust variations to achieve the commanded flight altitudes.

Fig. 21 demonstrates the results of the flight tests of the controller for the lateral motion. The deviations Δy commanded by the controller are indicated and it is evident, that the actual distances in lateral direction agree very well with the prescribed values. The deviation from the commanded position line are within 5m. This result has been achieved, although there was some turbulence during that flight. Rudder and aileron deflections show a small offset which compensates the moments due to the spin of the propellers. The heading follows the commanded value. Finally it can be stated, that the controller is able to hold the aircraft on a prescribed position line which is a necessary condition for formation flights.

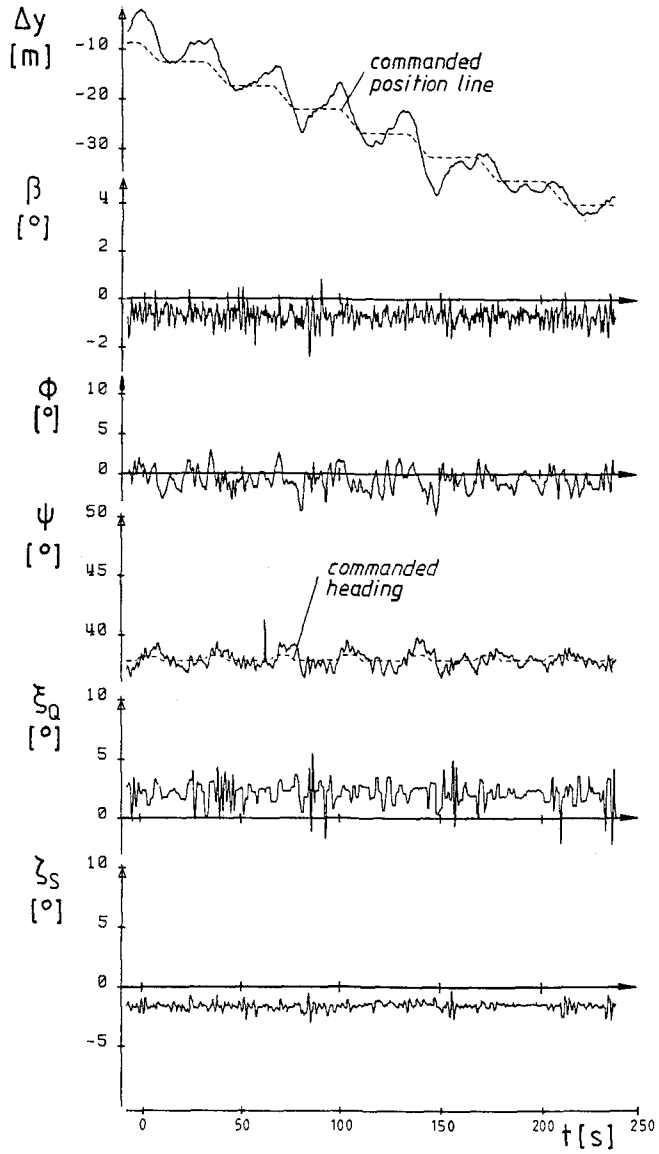

Fig. 21: Behaviour of the lateral part of the flight controller in single flight during flight tests of an airplane DO-28.

5.4.2 Behaviour in formation flights

After successful testing of the formation flight controller in single flight, some formation testing has been carried out. Fig. 22 shows a typical result. The longitudinal distance of the rear airplane relative to the leading airplane was ap-

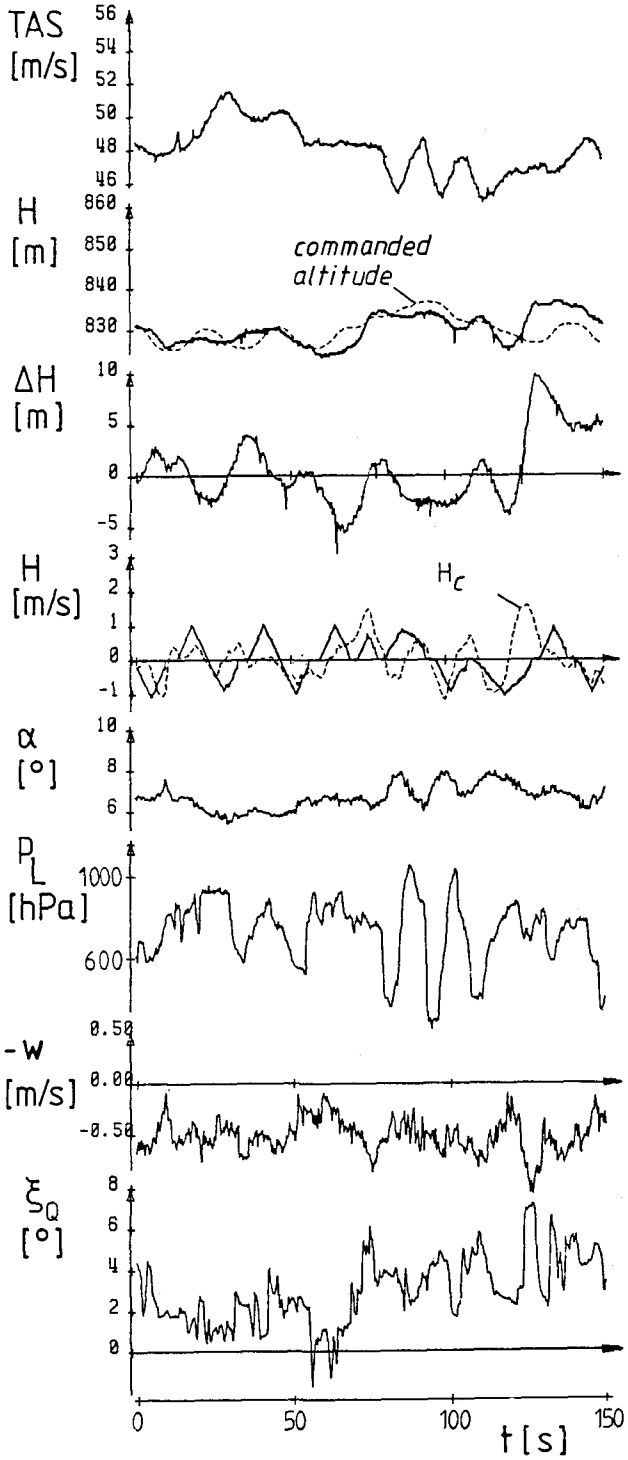

Fig. 22: Behaviour of the longitudinal part of the flight controller in formation flight during flight tests with two airplanes (DO-228 and DO-28).

proximately three wing spans and an average lift coefficient of c_L = 0.875 has been evaluated for that flight. The commanded altitude steps and the variations of the climb rate can be easily read off the time history for the flight altitude $\dot{H}$ = dH/dt and the vertical speed H and simultaneously it is evident, that the commanded values are in good agreement with the actual states. The air speed shows some variations. Since the air speed is used to fix the longitudinal distance, corresponding variations of this distance should be expected. But the evaluation of the photographs taken during the formation flights showed for the time inverval under consideration only variations within one semi span. The most important variables in formation flight are aileron deflections and induced upwash velocity, because they are direct measures for the achieved power reduction, see section 5.2.4. Fig. 22 indicates that large aileron deflections are combined with large upwash velocities at all times. This confirms the assumption, that the aileron deflections are a very good sensor for the induced upwash velocity along the wing span. There is not such a clear correlation for the measured manifold pressure. This is due to the fact, that the manifold pressure contains all variations necessary for the control of the air speed and for the commanded position.

5.5 Power reduction with automatic control system

The main reason for formation flights is the achievable power reduction. As an outcome from Fig. 22, large induced upwash velocities and aileron deflections have been measured, indicating a power reduction. Therefore the power reduction was evaluated for the time interval of Fig. 22, using the method according to section 4.2. The result is shown in Fig. 23. As a scaling factor, the maximum theoretical power reduction for this formation at the optimum position is included. The power reduction was evaluated for those moments of time, when the controller measured the induced upwash, the manifold pressure and the aileron deflections in order to decide which size and direction the next step in search for the maximum should have. Within the time interval under consideration power reductions were obtained, which reached maximum values of more than 20%. The average value of the power reduction for the whole time interval has been evaluated as e_2 = 10.24%. This value is also included as dashed line in Fig. 23.

In addition the power reduction was calculated from the simulation test of section 5.3. Thereby the method of section 4.2 was used to evaluate the power reduction, and a value e_2 = 8 % has been obtained for the rear aircraft in a flight formation of two equal aircraft DO-28. This result contains all losses due to the motion in search for the maximum. A slightly higher power reduction can be expected, if the front airplane is larger than the rear aircraft. In fact, as a result from the formation flight tests with the larger and heavier DO-228 as front airplane a power reduction of e_2 = 10.24 % was obtained. This leads to the conclusion that good agreement exists between the simulation tests and the real formation flight tests.

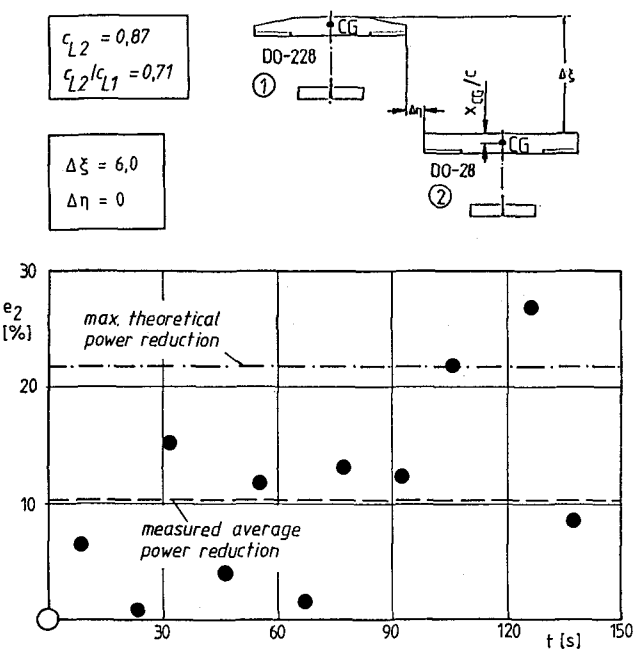

Fig. 23: Measured flight power reduction in autopilot-controlled formation flight with two airplanes (DO-228 and DO-28). Comparison between theory and experiment.

6. Conclusions

In the first part of this paper different methods of theoretical aerodynamics were applied to calculate the power reduction of flight formations. Methods using a simple horse-shoe vortex model are compared with methods using a plane or a rolled-up vortex sheet. With the simple horse-shoe vortex method, the power reduction of even large formations can be estimated quite easily. The power reduction is smaller then the one obtained from calculations with a plane or a rolled-up vortex sheet. Taking into account the complicated geometry of a rolled-up vortex sheet, slightly different power reductions are calculated compared with the results for unrolled plane vortex sheets. The power reduction has been calculated also for whole aircrafts. Thereby wings and tails have been taken into account. For each airplane the pitching moment about the center of gravity was balanced by means of elevator deflections of the whole horizontal tail and the rolling moments were compensated by means of aileron deflections. The resulting yawing moment again has been balanced by corresponding rudder deflections. These results show that there is only a minor influence from the consideration of these details. Power reductions of 15% are obtainable for the rear aircraft in formations of two equal airplanes at the same altitude and small spanwise distances. The aileron and rudder deflec-

tion for the compensation of the corresponding moments are of moderate size.

In the second part the performance characteristics have been measured in flight tests for formations of two airplanes DO-28 and compared with theoretical values. Excellent agreement was found for the obtainable power reduction and the corresponding aileron deflections for different positions of the two airplanes relative to each other. The flight tests have demonstrated that the power reduction can be realized in practical flight formations of two airplanes.

On the other hand the pilot of the rear airplane had some difficulties to maintain simultaneously the proper flight conditions and the proper position relative to the wake of the front airplane. To overcome these problems, a control system has been adapted for the rear airplane.

In a first step theoretical investigations based on the linearized differential equation of the aircraft motion have been carried out. The basic controllers for the lateral and longitudinal motion have been realized as state feed back controllers. The essential formation flight controller works as an extremum controller. The results of the simulation tests showed, that such a controller is always able to find and hold favourable positions in a flight formation. Beside the losses due to the application of an extremum controller, large power reductions up to 10% were achieved in a simulation for a formation of two equal airplanes.

Finally this controller has been implemented and tested on board a research airplane of the Technische Universität Braunschweig. Preliminary tests in single flight confirmed the proper function of the basic controllers for the longitudinal and lateral aircraft motions. The formation flights have been carried out in cooperation with Deutsche Forschungsanstalt für Luft- und Raumfahrt. An aircraft of type DO-228 was used as front airplane. The formation flight controller showed an acceptable behaviour during formation flight tests. In most cases a favourable position relative to the wake of the leading airplane could be found and held. Using the described formation flight controller power reductions up to 10% could be obtained during flight tests and good agreement with theoretical values turned out. Thus, it has been shown that formation flights can be realized successfully with an extremum flight controller.

References

[1] D. Hummel: Aerodynamic aspects of formation flight in birds. J. theor. Biol. 104 (1983), 321 - 347.

[2] C. Wieselsberger: Beitrag zur Erklärung des Winkelfluges einiger Zugvögel. Z. Flugtechnik u. Motorluftschiffahrt 5 (1914), 225 - 229.

[3] H. Schlichting, E. Truckenbrodt: Aerodynamics of the Airplane. Mc Graw-Hill, New York, 1979.

[4] H. Schlichting: Leistungsersparnis im Verbandsflug. Mitt. dt. Akad. Luftfahrtforsch., H.2 (1942), 97 - 139. See also: Jb. 1942/43 dt. Adad. Luftfahrtforsch., 546 - 554.

[5] P. B. S. Lissaman, C. A. Schollenberger: Formation flight of birds. Science 168 (1970), 1003 - 1005.

[6] D. Hummel: Die Leistungsersparnis beim Verbandsflug. J. Orn. 114 (1973), 259 - 282.

[7] D. Hummel: Die Leistungsersparnis in Flugformationen von Vögeln mit Unterschieden in Größe, Form und Gewicht. J. Orn. 119 (1978), 52 - 73.

[8] D. Hummel: Recent aerodynamic contributions to problems of bird flight. Proc. 11th Congr. Int. Council Aerospace Sci. (ICAS), Lisbon 1978, Vol. 1, 115 - 129.

[9] D. Hummel, K.-W. Bock: Leistungsersparnis durch Formationsflug. Z. Flugwiss. Weltraumforsch. 5 (1981), 148 - 162.

[10] M. Beukenberg, D. Hummel: Flugversuche zur Messung der Leistungsersparnis im Verbandsflug. Jb. dt. Ges. Luft- und Raumfahrt (DGLR) 1986, Bd. 1, 133 - 145.

[11] D. Hummel, M. Beukenberg: Aerodynamische Interferenzeffekte beim Formationsflug von Vögeln. J. Orn. 130 (1989), 15 - 24.

[12] A. Redeker: Beiträge zur Verbesserung der Führungsgenauigkeit von Flugreglern. Dissertation TU Braunschweig 1986.

[13] A. Redeker: Computer-aided flight testing of a digital autopilot on board a research aircraft. Proc. 14th Congr. Int. Council Aerospace Sci. (ICAS), Toulouse 1984, Vol. 1, 669 - 677.

[14] K. Gersten: Über die Berechnung des induzierten Geschwindigkeitsfeldes von Tragflügeln. Dissertation TH Braunschweig 1957. Jb. 1957 Wiss. Ges. Luftfahrt (WGL), 172 - 190.

[15] M. Beukenberg: Beiträge zu Aerodynamik und Flugmechanik des Formationsfluges. Dissertation TU Braunschweig 1989.

[16] L. L. Gould, F. Heppner: The vee formation of Canada Geese. Auk 91 (1974), 494 - 506.

[17] S. Schindler: Über den Zug des Kranichs (Grus grus) durch die Lüneburger Heide. Celler Ber. Vogelkde. 2 (1972).

[18] C. Urban, R. Behr, S. Wagner: Berechnung nichtlinearer aerodynamischer Charakteristika von interferierenden Tragflächen mittels eines Wirbelgitterverfahrens bei Unterschallströmung. DGLR-Bericht 86-3 (1986), 303 - 316.

[19] M. M. Munk: Isoperimetrische Aufgaben aus der Theorie des Fluges. Dissertation Uni. Göttingen 1919.

[20] H.G. Jacob: Rechnergestützte Optimierung statischer und dynamischer Prozesse. Springer Verlag, Berlin, Heidelberg, New York, 1982.

[21] W. Kaufmann: Über die Ausbreitung kreiszylindrischer Wirbel in zähen (viskosen) Flüssigkeiten. Ing. Arch. 31 (1962), 1-9.

[22] K. Kirde: Untersuchungen über die zeitliche Weiterentwicklung eines Wirbels mit vorgegebener Anfangsverteilung. Ing. Arch. 31 (1962), 385-404.

[23] A. Betz: Verhalten von Wirbelsystemen. ZAMM 12 (1932), 164-174.

[24] P.Vörsmann: Ein Beitrag zur bordautonomen Windmessung. Diss. TU Braunschweig 1985.